

Magma Emplacement and Remobilization Timescales Beneath Montserrat: Insights from Sr and Ba Zonation in Plagioclase Phenocrysts

G. F. ZELLMER^{1*}, R. S. J. SPARKS¹, C. J. HAWKESWORTH¹ AND M. WIEDENBECK²

¹DEPARTMENT OF EARTH SCIENCES, UNIVERSITY OF BRISTOL, WILLS MEMORIAL BUILDING, QUEENS ROAD, BRISTOL BS8 1RJ, UK

²GEOFORSCHUNGSZENTRUM POTSDAM, PROJEKTBEREICH 4.2, TELEGRAFENBERG, 14473 POTSDAM, GERMANY

RECEIVED NOVEMBER 22, 2001; ACCEPTED DECEMBER 12, 2002

Since 1995, the Soufrière Hills volcano on Montserrat, Lesser Antilles island arc, has erupted crystal-rich andesite magma that is geochemically very similar to the volcanic products of at least the last 174 ± 3 kyr (1σ). Nomarski images of plagioclase phenocrysts from six andesites erupted between 151 ± 4 ka (1σ) and AD 1999 reveal multiple crystal resorption events, and major shifts in anorthite content suggest that these are due to temperature variations. A model is developed that uses partitioning data for Ba and Sr to quantify the degree of intracrystalline disequilibrium of these elements with respect to anorthite content in 12 selected plagioclase phenocrysts. Intracrystalline diffusive equilibration of both Ba and Sr profiles is incomplete. However, local disequilibria do not consistently decrease towards crystal cores, i.e. potential differences between core and rim ages cannot be resolved, and so the timescale for crystal growth is considerably shorter than their residence time at magmatic temperatures. Using two-dimensional finite difference modelling of intracrystalline Sr diffusion as a first-order approximation of diffusion in three dimensions, it is possible to calculate bulk crystal residence times at the estimated Soufrière Hills magmatic temperature of 850°C . These range from ~ 10 to ~ 1200 years, independent of eruption age. Crystal residence times in the currently erupting andesite range from ~ 15 to ~ 320 years. Diffusion in three dimensions would result in shorter residence times. Such results can be explained by repeated intrusion of small volumes of andesitic material to upper-crustal levels, followed by rapid crystallization during degassing and rapid cooling. Remobilization of the intruded andesites by influx of

hotter, more mafic magma, and amalgamation of andesites of different crystallization ages by associated convective processes, produced the currently erupting andesite that contains abundant inclusions of mafic magma. The short residence times of andesite magma in the upper crust, and the episodic character of volcanism at the Soufrière Hills with short periods of intense volcanism alternating with much longer periods of dormancy, are consistent with deep magma generation and storage and with episodic ascent to form ephemeral shallow chambers.

KEY WORDS: plagioclase; crystallization; trace element zonation; diffusion

INTRODUCTION

The timescales of petrogenetic processes such as fractional crystallization, crystal growth and crystal residence are critical for models of magma emplacement, remobilization, transport and eruption at active volcanic edifices (e.g. Higgins, 1996; Condomines, 1997; Zellmer *et al.*, 1999; Charlier & Zellmer, 2000; Hawkesworth *et al.*, 2001). Understanding the rates of such processes may provide important constraints for volcanic hazard assessment and mitigation. Here a technique is developed for determining plagioclase residence times at the Soufrière Hills volcano on

*Corresponding author. Present address: Lamont–Doherty Earth Observatory, 61 Route 9W, Palisades, NY 10964, USA. Telephone: +1-845-365-8907. Fax: +44-845-365-8155. E-mail: gzellmer@ldeo.columbia.edu

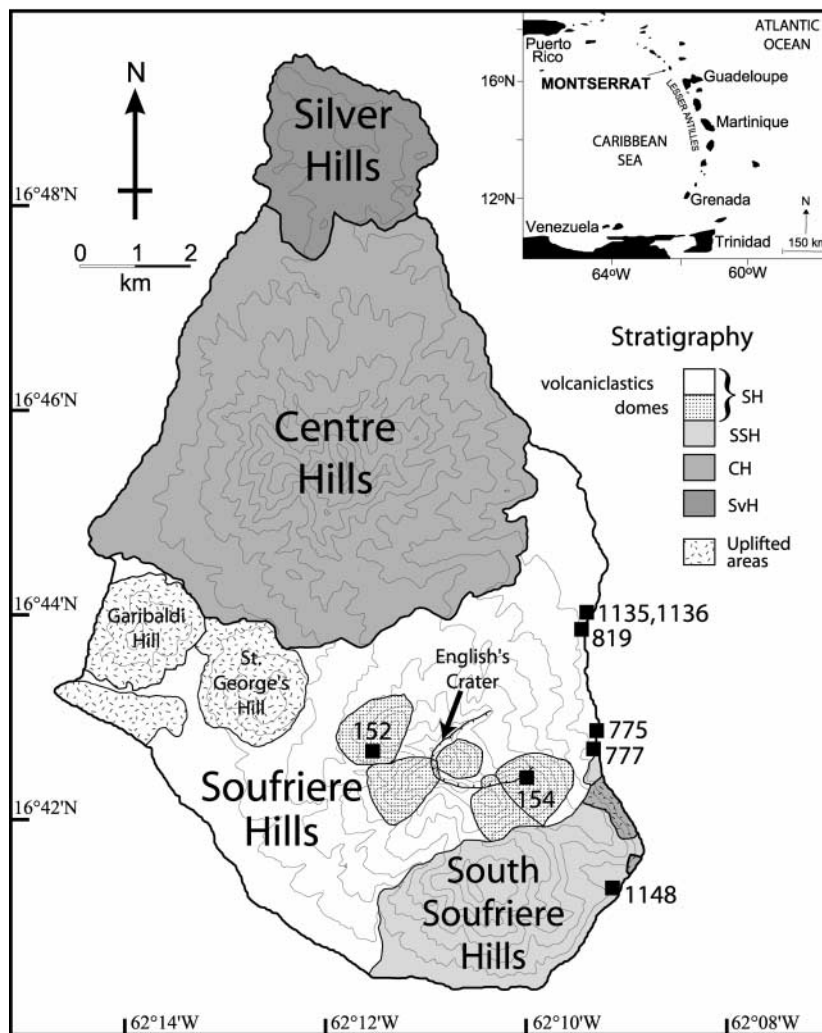


Fig. 1. Geological map of Montserrat, adapted from Harford *et al.* (2002). Inset: map of the Lesser Antilles arc.

Montserrat, West Indies, which started erupting andesitic lava in 1995. Since then, there has been much interest in the causes of the renewed activity and the petrogenesis of the andesitic magmas (Devine *et al.*, 1998; Murphy *et al.*, 2000), and the data presented here provide further insights into the magmatic processes beneath this active arc volcano.

The island of Montserrat (16.7°N, 62.2°W) is situated in the northern part of the ~750 km long Lesser Antilles island arc, which formed by westward subduction of the Atlantic oceanic lithosphere beneath the Caribbean Plate. A geological map of the island, based on the stratigraphy and ³⁹Ar/⁴⁰Ar dating of Harford *et al.* (2002), is given in Fig. 1. The Silver Hills, in the northern part of the island, represent the oldest volcanic centres (>1000 ka). The Centre Hills volcanic centres range in age from ~1000 ka to ~500 ka. Southern Montserrat is formed by the mafic

South Soufrière Hills complex (~130 ka) and by the Soufrière Hills andesite volcano (~300 ka to present). The flanks of the Soufrière Hills volcano are composed of pyroclastic deposits, and its core is formed by andesitic lava domes.

The andesites of the current eruption are very similar in mineralogy and geochemistry to the products of previous eruptions, and contain abundant inclusions of mafic magma that show evidence for having been molten when incorporated into the andesite (Murphy *et al.*, 1998). The eruption was preceded by a period of seismic swarms, which began in early 1992. Periods of seismic crises have previously occurred on the island in 1896–1897, 1932–1935 and 1966–1967 (Powell, 1938; Perret, 1939; Shepherd *et al.*, 1971), but none of these led to eruption.

Here, plagioclase major and trace element profiles are used to constrain the degree of post-crystallization

Table 1: Summary information on the studied plagioclase crystals

Plagioclase phenocryst	Eruption age	Standard deviation of Sr data around mean (%)	Crystal residence time (years)* at		
			800°C	850°C	900°C
<i>Prehistoric Soufrière Hills</i>					
MVO 152-p1	151 ± 4 ka†	4.8	4160	1220	395
MVO 152-p7	151 ± 4 ka†	8.1	1150	330	105
MVO 777-p6	75 ± 10 ka†	5.7	1270	350	110
MVO 777-p7	75 ± 10 ka†	4.7	3630	1030	325
MVO 775-p3	24 ± 1 ka†	3.8	2020	550	170
MVO 775-p5	24 ± 1 ka†	3.5	32	9	3
MVO 1135-p8	~19.7 ka‡	4.0	390	110	35
<i>Current eruption</i>					
MVO 1122-p5	AD 1999§	3.2	60	17	5
MVO 1122-p8	AD 1999§	4.5	1080	320	105
MVO 1151-p3	AD 1999§	5.3	650	190	65
MVO 1151-p5	AD 1999§	5.3	220	65	22
MVO 1151-p6	AD 1999§	3.8	980	275	85

*Accurate to a factor of ~2 owing to uncertainty in the diffusion coefficient (see Giletti & Casserly, 1994).

†Ar–Ar dates of Harford *et al.* (2002), with 1 σ error.

‡Collected by G. Zellmer from ¹⁴C-dated subunit III of Roobol & Smith (1998).

§Collected by the MVO shortly after eruption.

disequilibrium of the trace element distribution with respect to anorthite content. Then, crystal residence times are calculated from finite difference modelling of Sr diffusion within plagioclase, and the results are used to put constraints on the periodicity of magma emplacement and remobilization beneath Montserrat. Samples used include material from both prehistoric volcanic rocks and the dome of the current eruption (Table 1). Twelve crystals were selected from andesites with six different ages, encompassing samples that include several of the major dome-forming events of the Soufrière Hills volcano.

ANALYTICAL TECHNIQUES

Nomarski imaging was performed at Geneva University using standard techniques. Electron microprobe analyses on carbon-coated polished thin sections were performed at Bristol University on a JEOL JXA-8600 four-spectrometer instrument with LINK analytical X-ray analysis system and LEMAS automation. Online data reduction used the ZAF model. Run conditions were 15–20 kV accelerating voltage and 5 nA beam current with a beam diameter of 1–5 μ m.

Ion microprobe measurements were made on gold-coated polished thin sections using the Cameca ims-4f at Edinburgh University and the Cameca ims-6f at the GeoForschungsZentrum Potsdam. On the Edinburgh

instrument, a ¹⁶O[−] primary beam of 15 keV net energy and 5–9 nA beam current was used to sputter pits of ~15 μ m diameter. Positive secondary ions were accelerated through 4.5 keV into a double focusing mass spectrometer. Molecular ions were suppressed by use of energy filtering techniques (Zinner & Crozaz, 1986), using a 40 V energy bandpass to which a 75 V offset voltage was applied. Intensities for each element were measured on the electron multiplier at a single isotope in order of increasing mass, for between 2 and 8 s per peak, over 10 cycles. Element concentrations were calibrated using a combination of feldspar (SHF-1, Hill-32, Lake County) and borosilicate glass standards. Their ion yields had patterns similar to NBS SRM 610 (Hinton, 1990), but their overall ionization efficiency relative to Si was 15–30% lower. This is consistent with previous measurements of these reference samples.

The Potsdam instrument was operated at low mass resolution ($M/dM = 300$) with a nominal accelerating voltage of 10 kV and a 2 nA ¹⁶O[−] primary beam, sputtering pits of ~15 μ m diameter. The mass spectrometer was set for a 50 V energy bandpass to which a 60 V offset voltage was applied. Intensities were measured for 2 s per peak over 16 cycles. Multiple isotopes of the heavier elements were analysed to assess the presence of molecular interferences within the mass spectrum. Element concentrations were referenced to a gem labradorite AMNH 95557.

Relative sensitivity factors (RSF) were calculated for each element using the average of the standard analyses. For example, the RSF for Sr was calculated from $RSF_{Sr} = (^{88}Sr^{+}/^{30}Si^{+})_{std}/(Sr/SiO_2)_{std}$. The Sr concentration of the sample was then determined by $Sr_{sample} = [(^{88}Sr^{+}/^{30}Si^{+})_{sample}(SiO_2)_{sample}]/RSF_{Sr}$, where the SiO_2 content at a given domain in the sample had been determined earlier by electron probe. Absolute element concentrations are accurate to better than 10% (1σ), but relative variations in concentration across a single crystal could be resolved to better than 2% (1σ).

PLAGIOCLASE ZONING PATTERNS

Nomarski studies

Nomarski interference contrast imaging is a powerful technique for visualizing zoning patterns in igneous plagioclase crystals (Anderson, 1983). Nomarski images of typical Montserrat plagioclase phenocrysts are given in Fig. 2. They reveal (1) crystal growth zones with abundant melt pockets that were included into the crystal during growth, (2) multiple resorption surfaces characterized by rounded edges and truncation of growth surfaces, (3) zones of partial resorption (sieve-textures), also noted by Stewart & Fowler (2001), and (4) multiple zones of partial resorption. Single large zones of partial resorption may be a sectioning artefact. Resorption surfaces and zones of partial resorption may also be intimately associated as in Fig. 2e, suggesting that they are formed by the same process. Resorption features are common in andesitic plagioclases and have long been recognized (e.g. Pailuc, 1932).

To illustrate the intensive variables that control crystal growth and resorption, the plagioclase phase diagram, adapted from Yoder *et al.* (1957) and Housh & Luhr (1991), is shown in Fig. 2f for an H_2O -saturated andesite at 2 kbar. The position of the phase boundaries is a function of total pressure, P_{total} , and water pressure, P_{H_2O} , where the control of P_{H_2O} is dominant. In H_2O -undersaturated systems, decompression will result in superheating and resorption as the liquidus temperatures falls with decreasing P_{total} . As H_2O -saturation is reached ($P_{H_2O} = P_{total}$), further decompression will result in degassing, undercooling and crystal growth as the liquidus temperature rises with decreasing P_{H_2O} . Crystal growth can thus be caused not only by cooling, but also by degassing in response to decompression. Conversely, heating is one of the few viable mechanisms to produce resorption or partial resorption (sieve textures) in H_2O -saturated systems, although changes of the non-volatile melt composition, typically associated with magma mixing and rising temperature, can also have such effects.

Complex plagioclase growth histories, as revealed by Nomarski differential interference contrast (NDIC)

imaging, have commonly been attributed to processes that take place in the magma chamber or during magma ascent. Magma chamber processes include convection, in which individual crystals experience P , T and perhaps P_{H_2O} fluctuations as they are convected around the chamber, resulting in repeated weak dissolution and overgrowth (Singer *et al.*, 1993, 1995). Open-system processes may also be important, e.g. mixing of hot, more mafic magma with the resident magma, resulting in resorption surfaces associated with abrupt shifts in crystal composition (Stamatelopoulou-Seymour *et al.*, 1990; Singer *et al.*, 1995) or influx of volatiles, e.g. from mafic magma ponded at the base of the chamber (Couch *et al.*, 2001). Pressure variations can be produced in magma chambers by a variety of processes. In mechanically closed systems, containing volatile-saturated magma, water pressure increases as crystallization proceeds (Tait *et al.*, 1989). Likewise replenishment of magma chambers can increase pressure. However, in open systems pressure can decrease during eruptions as a result of removal of magma. Recent studies of periodic behaviour in volcanic eruptions (Barmin *et al.*, 2002) suggest that pressure fluctuations in chambers can be complex, and this may be reflected in correspondingly complex growth patterns in plagioclase. During magma ascent the solubility of H_2O in the melt decreases (e.g. Burnham, 1975), and for water-saturated magma the most important effect is thus likely to be exsolution of H_2O -rich gas, which can result in substantial crystallization (Blundy & Cashman, 2001). Associated crystal textures include oscillatory zoning in response to decompression pulses (Anderson, 1984), and zones rich in melt and fluid inclusions, which have previously been interpreted to result from rapid decompression (Singer *et al.*, 1993).

In Montserrat, the large number of resorption events recorded by some crystals points to complex crystallization histories, although changes in P - T conditions and volatile content were in many cases subtle, resulting in zones of partial resorption (sieve textures). Whether changes in pressure or temperature, P_{H_2O} fluctuations, or melt composition were dominant during crystallization and resorption cannot be constrained from NDIC imaging alone. The major and trace element geochemistry of the phenocrysts, and the timing of crystallization episodes, may be the key to resolving these questions.

Plagioclase compositions

Selected plagioclase crystals imaged by Nomarski techniques have been analysed by electron microprobe to produce detailed composition profiles and to characterize prominent internal boundaries identified by Nomarski imaging. These data are shown in

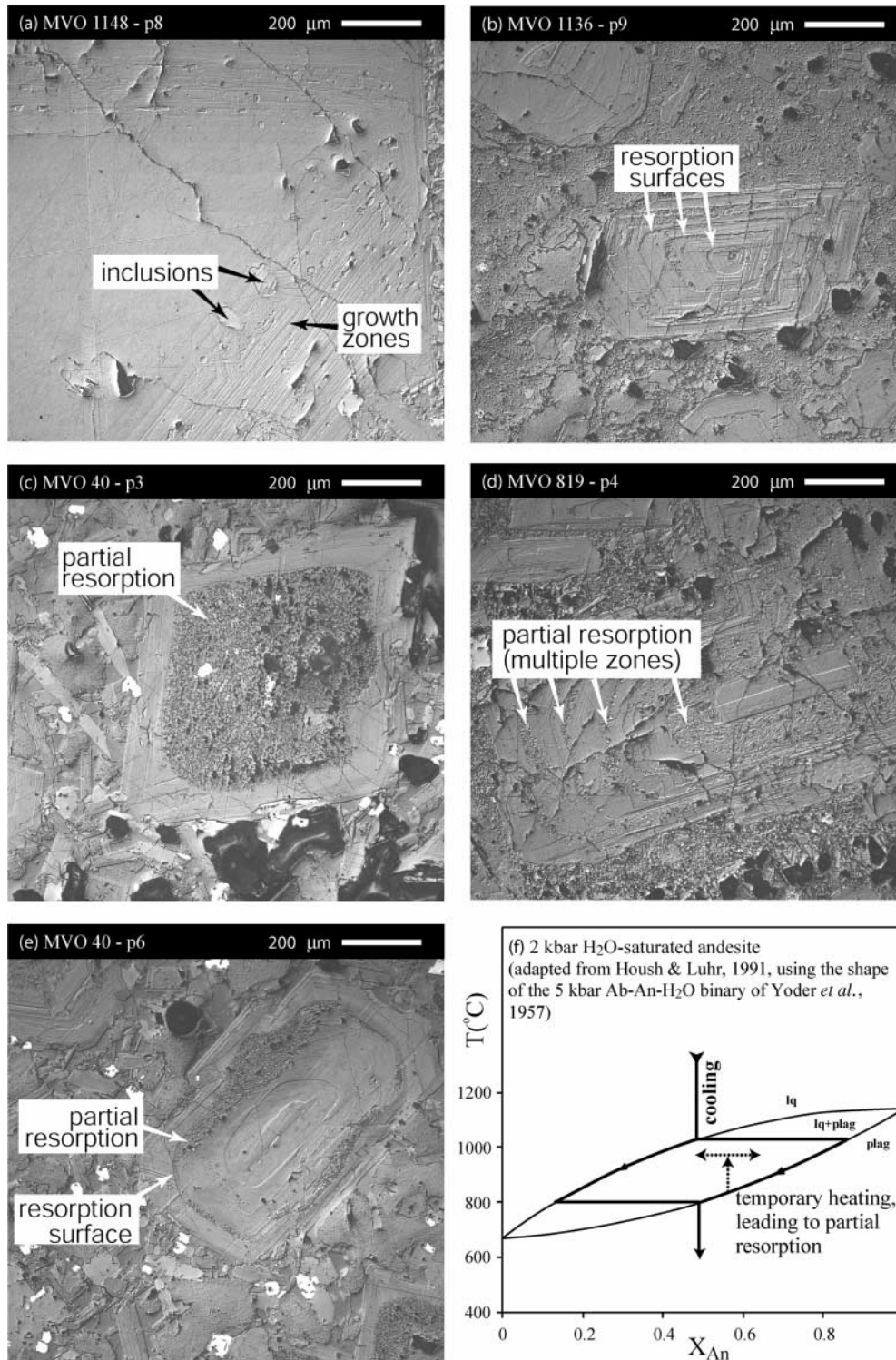


Fig. 2. (a–e) Nomarski images of Montserrat plagioclase phenocrysts. The following features are indicated by arrows. (a) Crystal growth zones with abundant melt inclusions. (b) Multiple resorption surfaces revealed by rounded edges and truncation of growth surfaces. (c) Large zones of partial resorption. (d) Multiple zones of partial resorption. (e) Resorption surfaces and zones of partial resorption that are intimately associated. (f) Plagioclase phase diagram relevant to an H₂O-saturated andesite at 2 kbar, adapted from Yoder *et al.* (1957) and Housh & Luhr (1991). X_{An} in this multi-component system is calculated as $An/(An + Ab)$. The effects of temperature changes are indicated. (See text for details on the effects of changing P_{total} and P_{H_2O} .)

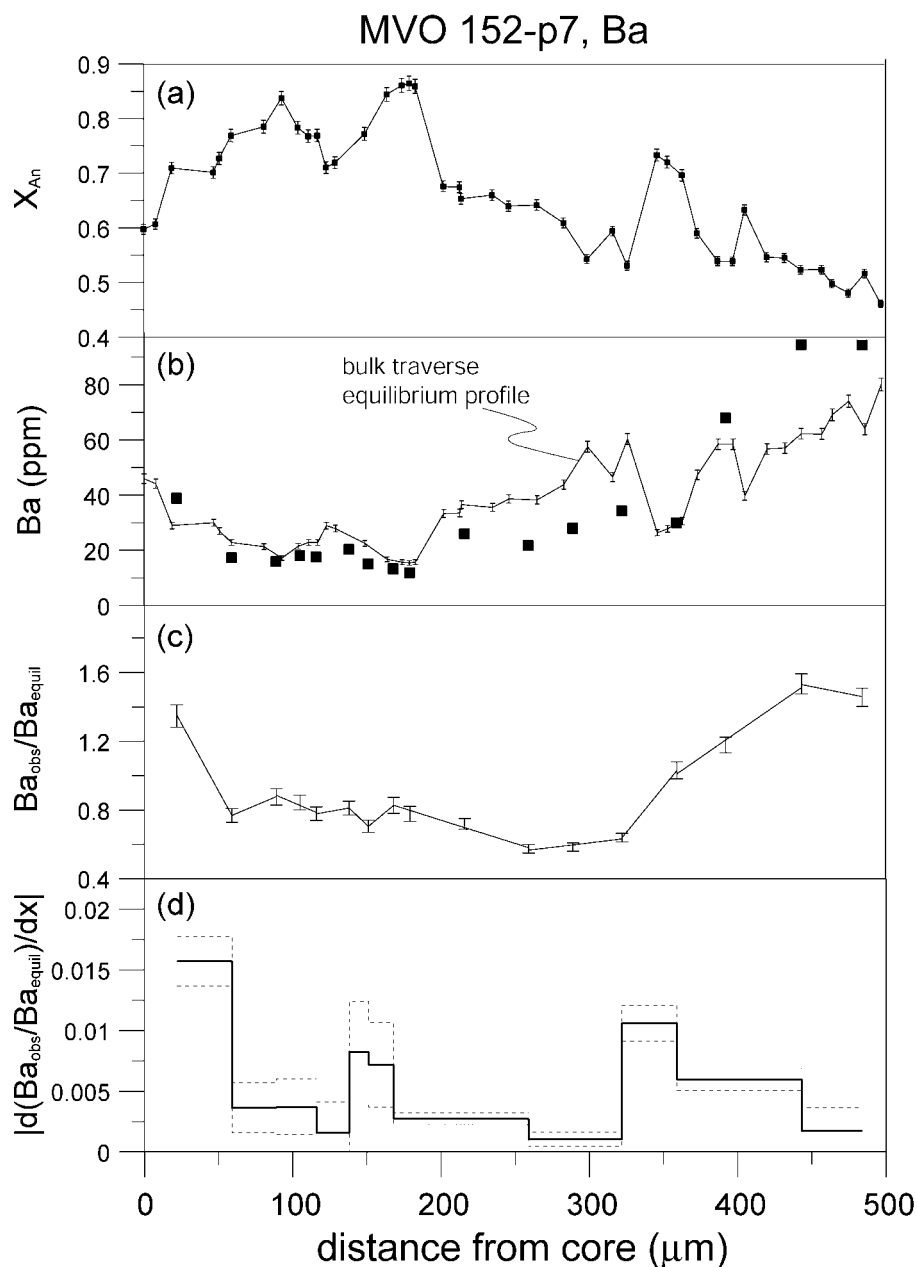


Fig. 3. Assessing intracrystalline Ba disequilibria of plagioclase crystal MVO 152-p7. Observations are given as filled squares. From the anorthite content measured by electron microprobe (a), a bulk traverse equilibrium Ba profile has been calculated and compared with the observed Ba profile, measured by ion microprobe (b). The ratios of observed and bulk traverse equilibrium concentrations (c) provide insights into local disequilibrium between individual zones. Adjacent zones are in local equilibrium where the profile in (c) is flat. Slopes in this profile are obtained from a series of linear regressions through Ba_{obs}/Ba_{equil} , and their absolute values are given in (d) as a measure of local disequilibrium (continuous line), together with their 95% confidence limits (dashed lines). Zones of linear regressions were chosen so that the errors were minimized. Local equilibrium is reached where $|d(Ba_{obs}/Ba_{equil})/dx| = 0$.

Figs 3 and 4; they include examples from prehistoric Montserrat lavas as well as lava from the current eruption. The complete dataset (Electronic Appendix 1) may be downloaded from *Journal of Petrology* Online at <http://www.petrology.oupjournals.org/>. The range of zoning patterns, internal textures and compositions

are in general similar to those identified by Murphy *et al.* (2000). A wide range of patterns is apparent in a single thin section, consistent with the concept that feldspars with very different crystallization histories have been mixed together. Taking the dataset as a whole, marked changes in An content are observed at

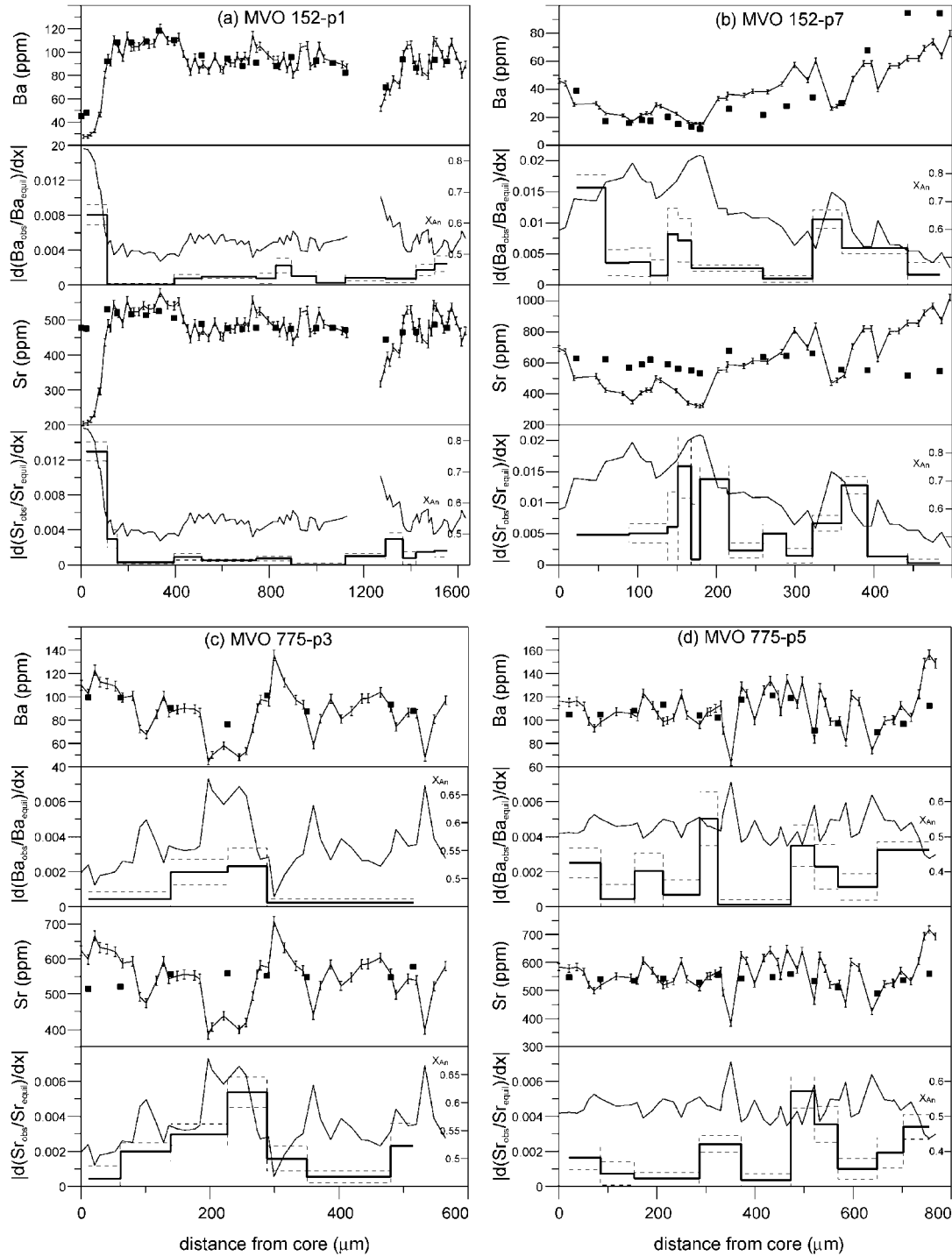


Fig. 4. (a–d)

major internal boundaries, with sharp increases in An content occurring outboard of major resorption surfaces and sieve-textured zones. Some crystals display complex fluctuations of An content, confirming the

observations of the Nomarski images and previous observations by Murphy *et al.* (2000).

Although only five crystals from two samples of the lava of the current eruption have been investigated

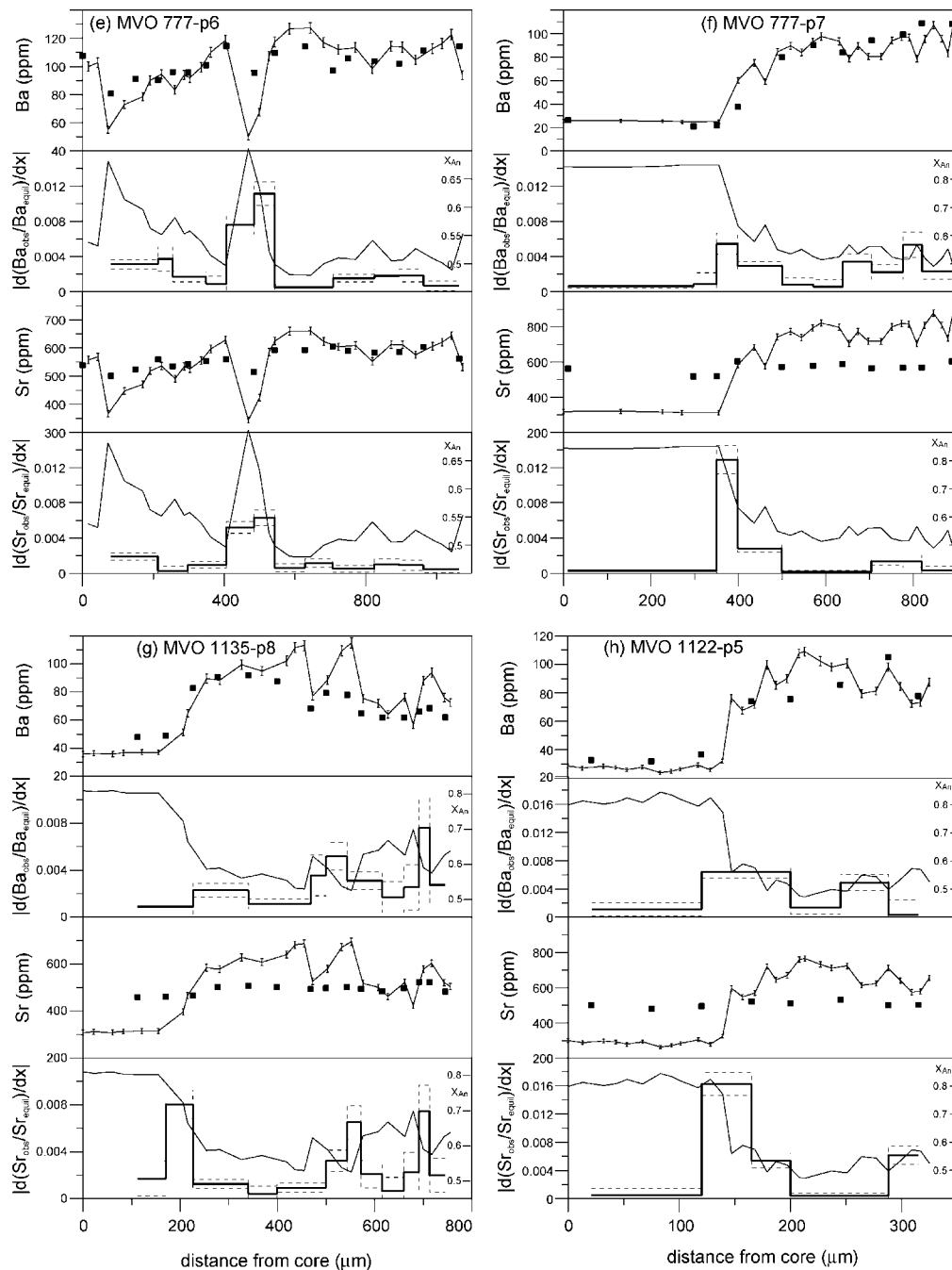


Fig. 4. (e-h)

here, some differences from the observations reported by Murphy *et al.* (2000) are apparent. In particular, MVO 1122-p5 (Fig. 4h) has a substantial homogeneous core of calcic feldspar ($An_{>80}$). There are other examples from older volcanic units of plagioclases with calcic (An_{70-90}) cores that in broad terms are normally zoned. Boundaries between calcic cores with more sodic overgrowth are generally sharp. Such calcic compositions require crystallization from a magma that

is either hotter or crystallized at much higher P_{H_2O} . Crystal cores may be restite from partial melting of the lower crust, remnants of an earlier phase of crystallization, or introduced into the andesite by mixing with mafic magma.

Crystal MVO 1151-p3 (Fig. 4j) is an example of the kind of crystal described as common by Murphy *et al.* (2000), with a large core of sodic feldspar (An_{50-60}) with weak and unsystematic zoning overgrown by a

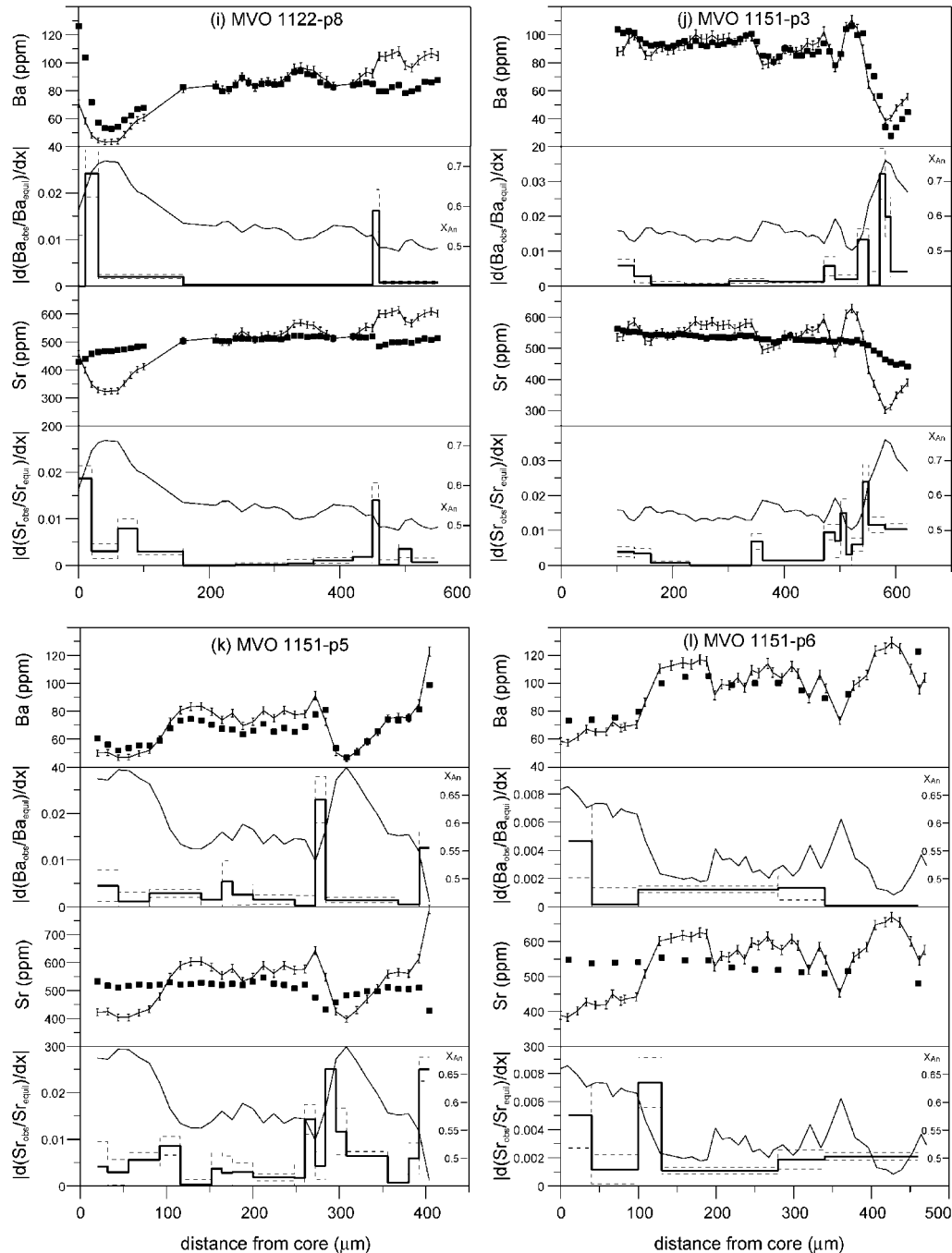


Fig. 4. Assessing bulk traverse and local disequilibria in Ba and Sr for 12 analysed plagioclase phenocrysts from Montserrat andesites. Observed and bulk traverse equilibrium profiles are given for both Ba and Sr (see Fig. 3b), and local disequilibria (see Fig. 3d) and X_{An} (see Fig. 3a) are combined in one diagram. It should be noted that observed trace element concentrations are indicated by filled symbols, and that the scale of X_{An} is given on the right of and inside each diagram. For profiles MVO 1122-p8, MVO 1151-p3 and MVO 1151-p5, anorthite content was calculated from the CaO content determined by the ion microprobe to ensure good spatial correspondence of X_{An} and trace element measurements, using the equation $X_{An} = 1 \times 10^{-4}CaO^2 + 4.74 \times 10^{-2}CaO$, where CaO is the CaO content in wt %.

thick rim of more calcic feldspar. Phase equilibria studies on Montserrat groundmass compositions show that relatively high magma temperatures of 900–1000°C are required to produce the observed calcic

overgrowth rims of up to An_{75} (Couch *et al.*, 2001). This would indicate that the rims formed in response to renewed crystallization subsequent to a rise in magma temperature. Such a temperature rise could

be the result of intrusion of a hotter mafic magma into the upper crust, evidenced by abundant mafic inclusions found in the andesites and by other petrological observations (Devine *et al.*, 1998; Murphy *et al.*, 2000).

Thus, whereas minor variations in X_{An} may be due to a number of different processes described in the previous section, major changes in X_{An} , as revealed by prominent boundaries in the Nomarski images, are thought to be dominated by variations in temperature. In the following, intracrystalline disequilibria of Sr and Ba profiles are assessed and modelled to put constraints on the timescales of these processes.

INTRACRYSTALLINE DISEQUILIBRIA OF PLAGIOCLASE Sr AND Ba PROFILES

Theory and approach

Figure 3a and b shows X_{An} and Ba trace element profiles across phenocryst MVO 152-p7, which will be used as an illustration. Equilibrium partitioning between any two zones i and j within the crystal is independent of the composition of the liquid the crystal grew from (Zellmer *et al.*, 1999), and is given by

$$D^{i/j} = \exp \left[\frac{w(X_{\text{An}}^i - X_{\text{An}}^j)}{RT} \right] \quad (1)$$

where $D^{i/j}$ is the partition coefficient of the trace element between i and j , X_{An} is the mole fraction of anorthite, R is the gas constant (8.3145 J/mol K), T is temperature, and w is a constant that depends on the particular trace element: $w_{\text{Ba}} = -38\,200 \pm 3200$ mol/J; $w_{\text{Sr}} = -26\,700 \pm 1900$ mol/J. Details on how equation (1) is obtained have been given by Zellmer *et al.* (1999). Conserving the total trace element content of the traverse (i.e. the average trace element concentration calculated after linear intrapolation between data points), a bulk traverse equilibrium profile can be calculated for any given X_{An} profile, using

$$D^{i/j} = \frac{C_{\text{equil}}^i}{C_{\text{equil}}^j} \quad (2)$$

where C_{equil} is the bulk traverse equilibrium concentration of a zone. Errors (designated by σ) in the measurement of anorthite content result in an error in the calculated bulk traverse equilibrium concentrations of the trace element, such that

$$\sigma_{C_{\text{equil}}} = C_{\text{equil}} \frac{w}{RT} \sigma_{X_{\text{An}}} \quad (3)$$

The bulk traverse equilibrium profile of Ba, and its associated errors, have been calculated in Fig. 3b, providing evidence for intracrystalline Ba disequilibrium.

It is worth noting that crystallization of a mineral in surface equilibrium with the surrounding liquid does not generally lead to intracrystalline trace element equilibrium. Whereas the crystal rim will be in equilibrium with the liquid, the uptake of trace elements into the crystal is dependent on the concentration of the trace element in the melt, and this will in most cases change during crystallization, thereby producing trace element disequilibria between adjacent growth zones.

Once the bulk traverse equilibrium profiles are calculated, the degree of local disequilibrium between adjacent zones of the traverse can be constrained. Adjacent zones i and j of the crystal are in equilibrium if

$$\frac{C_{\text{obs}}^i}{C_{\text{obs}}^j} = D^{i/j} \quad (4)$$

where C_{obs} denotes the observed concentration of the trace element.

Equations (2) and (4) can be combined and rearranged such that

$$\frac{C_{\text{obs}}^i}{C_{\text{equil}}^i} = \frac{C_{\text{obs}}^j}{C_{\text{equil}}^j} \quad (5)$$

Here, ρ is defined as the ratio between observed and equilibrium concentrations. Local equilibria are identified in zones of the crystal where the ρ profile, given for Ba in Fig. 3c, has no slope, i.e. where $d\rho/dx = 0$. The condition for bulk traverse equilibrium is $\rho = 1$ across the entire traverse. A series of linear regressions through the ρ profile can be used to minimize the average error of all calculated slopes (see Fig. 3c). The absolute values of these slopes, $|d\rho/dx|$, and their 95% confidence limits, are a useful measure of local trace element disequilibria within individual plagioclase crystals. For example, the degree of local Ba disequilibrium across crystal MVO 152-p7 varies from core to rim, with maxima at ~ 50 μm , 150 μm and 350 μm , a result not immediately apparent by simply comparing observed and bulk traverse equilibrium Ba profiles (see Fig. 3d).

Characterizing Sr and Ba disequilibria of Soufrière Hills plagioclase crystals

The degree of local disequilibrium of the Sr profile can be characterized in the same way as described in the previous section. In Fig. 4a–l, Sr and Ba disequilibria are characterized for 12 Soufrière Hills plagioclase crystals. Sr and Ba profiles are given in the same figure for better comparison, together with the distribution of local disequilibria and the X_{An} profile. The following observations can be made:

(1) Sr concentration profiles are relatively flat, with standard deviations varying between 3.1 and 5.7%

around the Sr average (except Fig. 4b: 8.1%). In contrast, Ba concentration profiles show a much greater variability, with standard deviations of 10–50% around the Ba average, and generally follow the calculated bulk traverse equilibrium profiles more closely (see Fig. 4a, c and f–i).

(2) With the exception of xenocrystic cores with An_{80} , which are locally equilibrated (see Fig. 4f–h), the degree of local disequilibrium, $d\rho/dx$, in the Sr and Ba trace element distribution is generally variable and without a clear trend across the crystals. Only crystal MVO 1151-p3 yields a systematic increase in local disequilibria towards its rim (Fig. 4j).

The origin of variable Ba profiles and flat Sr profiles: an *a posteriori* model

Using crystal MVO 152-p7 (see Fig. 4b) as an example, Ba and Sr concentrations are plotted against X_{An} in Fig. 5. Whereas Ba concentrations increase five-fold with decreasing X_{An} , approximately following the predicted bulk traverse equilibrium partitioning, Sr concentrations remain relatively constant and out of bulk traverse equilibrium. In the following, these data are modelled by assuming closed-system crystallization of plagioclase in response to cooling or degassing. The details of the model are described below.

Murphy *et al.* (2000) used single-pyroxene geothermometry of orthopyroxene phenocrysts to estimate magmatic temperatures of the Montserrat andesites. Orthopyroxene cores yielded an average temperature of $\sim 850^\circ\text{C}$, consistent with core temperatures of large titanomagnetite ($835\text{--}850^\circ\text{C}$) and ilmenite phenocrysts (Devine *et al.*, 1998, 2003). Reversely zoned orthopyroxene rims recorded temperatures up to $\sim 1050^\circ\text{C}$, and this is therefore the minimum liquidus temperature of the crystal-poor mafic magma now sampled as inclusions in the andesite. Barclay *et al.* (1998) estimated the minimum depth of the water-saturated magma chamber to be 5 km, equivalent to ~ 1.5 kbar. Using these boundary conditions, closed-system compositional evolution can be modelled for a plagioclase crystal growing from a melt of MVO 152 whole-rock composition (Zellmer *et al.*, 2003), with a normative plagioclase content of > 60 vol. %. Other Ca- and Na-bearing phases constitute < 10 vol. % of the phenocryst assemblage (Murphy *et al.*, 2000), and their contribution to the evolution of the liquid is thus restricted. Housh & Luhr's (1991) calibration of the plagioclase phase diagram in a multi-component H_2O -saturated system was used to calculate X_{An} for the liquid and the corresponding plagioclase, adopting the shape of the Yoder *et al.* (1957) 5 kbar Ab–An– H_2O system. Crystallization by both isobaric cooling from $> 1050^\circ\text{C}$ to $< 850^\circ\text{C}$ at ~ 1.5 kbar and degassing

by isothermal decompression from ~ 5 to ~ 1.5 kbar at 850°C have been modelled as end-member cases. Changes in Sr and Ba concentrations were calculated using the partition coefficients of Blundy & Wood (1991).

During fractional crystallization of plagioclase, D_{Ba} is less than unity throughout, resulting in an increase of Ba concentration in the liquid that is accompanied by a steady increase in the Ba concentration in the crystal. The initial Ba distribution closely follows its bulk traverse equilibrium distribution (Fig. 5a). In contrast, D_{Sr} is always greater than unity, resulting in a decrease of Sr concentration in the liquid. However, as D_{Sr} steadily increases with decreasing X_{An} , the decrease in the liquid is compensated by an increase in the proportion of Sr taken up into the growing crystal, such that the Sr concentration within the crystal remains approximately constant. Thus, the initial Sr distribution is only very weakly dependent on anorthite content, and the distribution of Sr caused by crystallization is therefore not in bulk traverse equilibrium (Fig. 5b).

Whereas closed-system fractional crystallization can account for constant Sr content, in the simplest scenario it would predict a continuous decrease in anorthite content and increase in Ba content from core to rim of each crystal. This is clearly not observed, and there is evidence for multiple zones and frequent recursions to calcic low-Ba plagioclase. Without relaxing the closed-system constraint, such patterns could be produced by episodic partial remelting of an andesitic crystal mush accompanied by movement of the crystals relative to their heterogeneous partial melt.

Petrogenetic implications

In the previous section it was shown that closed-system crystallization within the Montserrat andesite is a process that may produce relatively constant Sr concentrations within the crystals and greater bulk traverse disequilibrium of Sr concentration profiles relative to Ba, although the occurrence of local Ba disequilibria indicates that the initial Ba distribution does not perfectly match the bulk traverse equilibrium Ba profile. This contrast between the observed trace element distribution and both bulk traverse and local equilibrium distribution can be expected if crystal growth is fast compared with the timescale of intracrystalline diffusive equilibration of the trace elements.

The absence of any trend of increasing local disequilibria from core to rim of a crystal (see Fig. 4) suggests that core and rim ages are not distinguishable by diffusive equilibration of trace elements within the crystal during crystallization. If the rate of crystal growth was slow compared with the rate of intracrystalline trace element diffusion, crystal cores would have had significantly more time to equilibrate than crystal rims, and

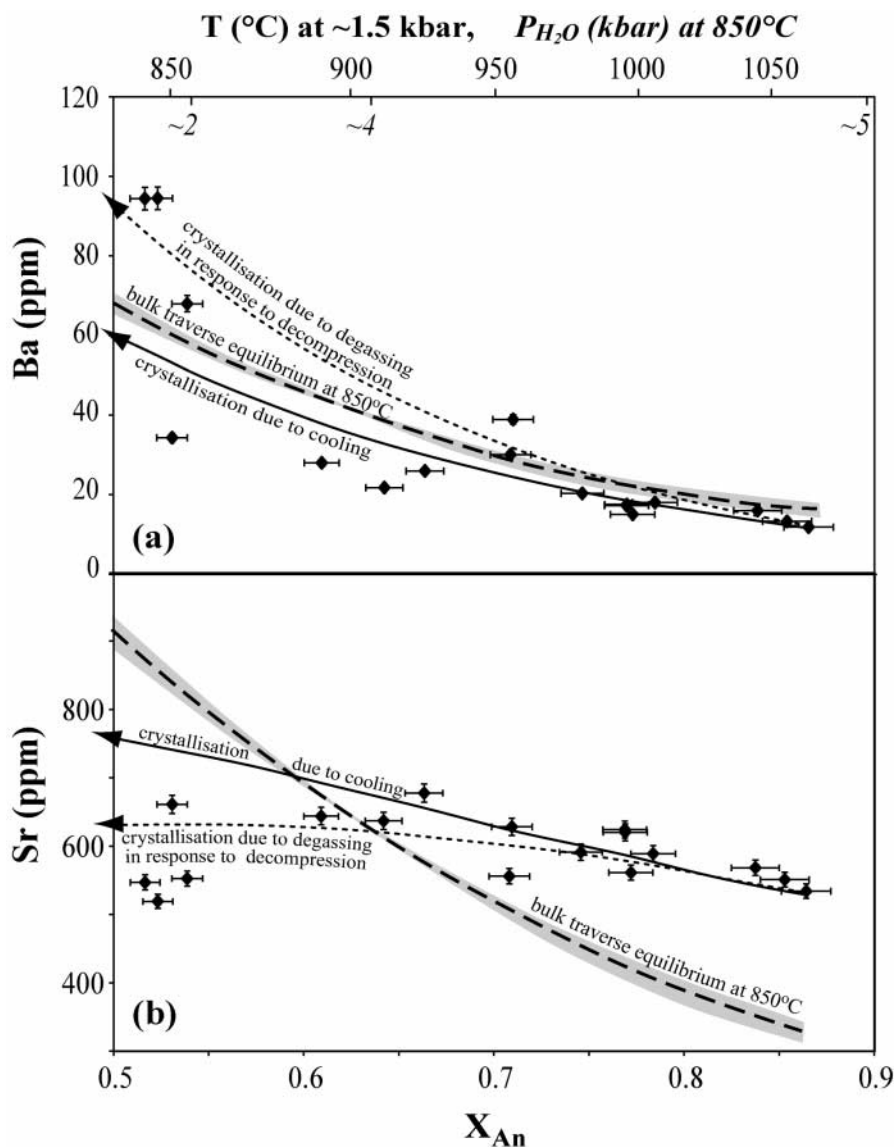


Fig. 5. Variation of (a) Ba and (b) Sr with X_{An} in plagioclase crystal MVO 152-p7. Compositions crystallized under H_2O -saturated conditions during isobaric cooling (continuous line) and during isothermal degassing in response to decompression at $850^\circ C$ (dotted line) are compared with compositions predicted by bulk traverse equilibrium partitioning (dashed line). The shaded area is the $\pm 2\sigma$ uncertainty range in the bulk traverse equilibrium partitioning as a result of the uncertainty in w in equation (1). (See text for details.) Initially flat Sr profiles are consistent with closed-system crystallization of plagioclase. Variations in Sr concentrations are likely to be due to subsequent diffusion, initially towards local equilibrium partitioning, and ultimately towards bulk traverse equilibrium partitioning (dashed line). The diffusive evolution of the Sr concentrations is complex because of the interplay between diffusion and partitioning as a function of local anorthite content (see inset to Fig. 7).

local trace element disequilibria would increase in magnitude from core to rim. This is not generally observed in crystals from Montserrat. Therefore, the timescale of crystal growth was short compared with the timescale of diffusive equilibration. By acknowledging that the initial Sr concentration profiles were relatively flat and independent of anorthite content, diffusion of Sr can be used to put constraints on the timescales of crystal growth and residence within the Soufrière Hills andesites at magmatic temperatures.

Finite element diffusion modelling is used in the next section to quantify these timescales.

DETERMINING PLAGIOCLASE RESIDENCE TIMES

Principles of Sr partitioning and diffusion in plagioclase

A full discussion of the principles of Sr partitioning and diffusion within plagioclase has been given by Zellmer

et al. (1999, and references therein). The main results are summarized in this section, together with an extended treatment of uncertainties and the effects of a third dimension.

Partitioning of Sr between plagioclase and liquid depends on the anorthite content, X_{An} (Blundy & Wood, 1991), and equilibrium partitioning between two parts i and j of a crystal is given by equation (1), above. Analytical errors in the measurement of anorthite content result in an error in the relative equilibrium partitioning, such that

$$\sigma_{D_{Sr}^{i/j}} = \frac{w_{Sr}}{RT} D_{Sr}^{i/j} \sqrt{\left(\sigma_{X_{An}^i}\right)^2 + \left(\sigma_{X_{An}^j}\right)^2}. \quad (6)$$

If C_{Sr}^i and C_{Sr}^j denote the measured concentrations of Sr in domains i and j of a crystal of plagioclase, respectively, then these concentrations can be considered in equilibrium at the 95% confidence limit (2σ) if

$$\left| \frac{C_{Sr}^i}{C_{Sr}^j} - D_{Sr}^{i/j} \right| \leq 2\sqrt{\left(\sigma_{(C_{Sr}^i/C_{Sr}^j)}\right)^2 + \left(\sigma_{D_{Sr}^{i/j}}\right)^2}. \quad (7)$$

If the Sr concentrations of adjacent zones within a plagioclase are not in equilibrium, as observed in crystals from the Soufrière Hills andesites, diffusion will occur to establish equilibrium. It should be noted that anorthite profiles are preserved, as coupled diffusion of Na, Ca, Al and Si is very slow (Morse, 1984) compared with diffusion of Sr (Cherniak & Watson, 1994; Giletti & Casserly, 1994). By modelling chemical diffusion of Sr, it is possible to calculate equilibration times for any pair of zones within a plagioclase crystal at a given temperature, i.e. the time required for equation (7) to be satisfied for two parts i and j of the crystal.

Trace element diffusion affects the calculation of intracrystalline equilibrium partitioning as a result of the three-dimensional nature of the crystal. For crystals that are not sectioned through their core and normal to their growth zones, the total trace element content of the traverse may not be conserved, because trace elements may diffuse into or out of the section from other parts of the crystal. In addition, trace element diffusion across the crystal–melt interface may change the total trace element content of the entire crystal. However, as the anorthite profile remains unchanged and $D^{i/j}$ in equation (2) therefore remains constant, trace element diffusion into or out of the section will change the bulk traverse equilibrium concentrations of all growth zones to the same degree. Thus, whereas the absolute magnitude of local disequilibria may change, their relative magnitude will be conserved along each traverse and the position of local equilibria will not change as $dp/dx = 0$ in zones

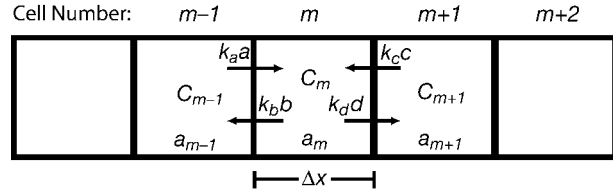


Fig. 6. Finite difference modelling of Sr diffusion in plagioclase. The change in concentration C in each cell m over time is calculated from the element fluxes $k_a a$ and $k_c c$ into the cell and $k_b b$ and $k_d d$ out of the cell, which depend on the diffusivities α .

of local equilibrium, independent of the absolute value of the bulk traverse equilibrium concentrations.

The diffusion coefficient of Sr in plagioclase, α_{Sr} , is governed by the exponential Arrhenius relationship, and is thus strongly dependent on temperature. The pre-exponential factor and the activation energy were calibrated by Giletti & Casserly (1994), who showed that the diffusion coefficient also depends on the anorthite content, and that

$$\alpha_{Sr} = 10^{-(4.1X_{An}+4.08)} \exp(-3.32 \times 10^4/T) \quad (8)$$

where the analytical uncertainty of α_{Sr} is approximately a factor of two at the $\pm 2\sigma$ level (Giletti & Casserly, 1994). Thus, plagioclase crystals have variable equilibrium partitioning and variable diffusivities. Analytical solutions for trace element diffusion within such media are not known. However, finite difference modelling can be used to model Sr diffusion within plagioclase crystals.

Finite difference modelling

A crystal may be modelled in two dimensions as a number of adjacent cells ($\dots, m-1, m, m+1, \dots$) of width Δx , each with its own diffusion coefficient α_m and its own Sr content C_m . As most secondary ionization mass spectrometry profiles are of lower spatial resolution, linear interpolation is used between measured X_{An} and Sr data points. Diffusion is modelled stepwise across the crystal, considering the diffusional exchange of Sr between three adjacent cells in a small time interval Δt . In detail, the diffusion of Sr into and out of cell m must be considered from and to both adjacent cells $m-1$ and $m+1$. This is illustrated in Fig. 6, where $k_a a$, $k_b b$, $k_c c$ and $k_d d$ are the element fluxes into and out of cell m , such that

$$C_m^{p+1} = C_m^p + k_a a - k_b b + k_c c - k_d d \quad (9)$$

where the superscripts designate the time increment.

In this equation, k_a , k_b , k_c and k_d are here referred to as flux factors. These depend on the equilibrium partitioning between the adjacent cells. In the case of *constant* equilibrium partitioning, the flux factors are equal to unity, and a and c are the element fluxes into

cell m , whereas b and d are the element fluxes out of cell m . Modifying the equations of Holman (1997) to take into account the fact that the rate of diffusion is controlled by the cell that has the lower diffusion coefficient of two adjacent cells, these fluxes are

$$a = \frac{\alpha_1 \Delta t}{(\Delta x)^2} C_{m-1}^p \quad (10)$$

$$b = \frac{\alpha_1 \Delta t}{(\Delta x)^2} C_m^p \quad (11)$$

$$c = \frac{\alpha_2 \Delta t}{(\Delta x)^2} C_{m+1}^p \quad (12)$$

$$d = \frac{\alpha_2 \Delta t}{(\Delta x)^2} C_m^p \quad (13)$$

where α_1 is the lower of the two diffusion coefficients α_m and α_{m-1} , α_2 is the lower of the two diffusion coefficients α_m and α_{m+1} , Δt is the time step from p to $p+1$, and Δx is the width of a cell. As a first-order approximation, the crystal is assumed to be a closed system, with no diffusion of trace elements into or out of the section.

In the case of *variable* partitioning, the flux factors are different from unity, because diffusivity applies to the chemical potential gradient, not the concentration gradient. For example, if in the case of *constant* equilibrium partitioning, cell $m+1$ has twice as much Sr as cell m , flux c is double flux d . In the case of *variable* equilibrium partitioning, however, if cell $m+1$ can accommodate twice as much Sr as cell m , k_d must be twice as high as k_c , so that in equilibrium the fluxes $k_c c$ and $k_d d$ are equal and cell $m+1$ retains twice as much Sr as cell m . Ensuring mass balance, the flux factors are then given by the following relations:

$$K_a = \left(\frac{C_m^{\text{equil}}}{2C_{m-1}^{\text{equil}}} + \frac{1}{2} \right) \quad (14)$$

$$K_b = \left(\frac{C_{m-1}^{\text{equil}}}{2C_m^{\text{equil}}} + \frac{1}{2} \right) \quad (15)$$

$$K_c = \left(\frac{C_m^{\text{equil}}}{2C_{m+1}^{\text{equil}}} + \frac{1}{2} \right) \quad (16)$$

$$K_d = \left(\frac{C_{m+1}^{\text{equil}}}{2C_m^{\text{equil}}} + \frac{1}{2} \right). \quad (17)$$

Finally, Δt must be chosen to be sufficiently small. In the one-dimensional system considered here, it can be shown (see Holman, 1997) that Δt must be smaller than or equal to Δt_{limit} , given by

$$\Delta t_{\text{limit}} = \frac{(\Delta x)^2}{2\alpha_{\text{highest}} k_{\text{highest}}} \quad (18)$$

where α_{highest} and k_{highest} are the highest diffusion coefficient and the highest flux factor for the modelled set of cells, respectively. The largest possible value of Δt was chosen to maximize processing speed. It was tested that the results of the method are independent of the time step.

Example: Sr diffusion in crystal MVO 152-p7

To elucidate the complexities of trace element diffusion in a system of variable equilibrium partitioning and variable diffusion coefficients, an example of closed-system diffusive modification of an initially flat Sr profile, as broadly inferred for the Soufrière Hills andesites (as in Fig. 5b), is given for crystal MVO 152-p7 at 850°C (Fig. 7). The calculated distribution of Sr within the crystal is indicated for 200 years and 3000 years residence time, and the bulk traverse equilibrium profile is also given. The calculation shows that the evolution of the Sr profile with time is complex, because of the interplay between diffusion and partitioning as a function of local variations in anorthite content. In particular, there are two non-intuitive features in the local evolution of Sr distribution. First, actual concentrations may overshoot or undershoot the bulk traverse equilibrium profile during diffusion, as can be observed in Fig. 7 at 359 μm , where the concentration of Sr, initially only ~ 100 ppm above bulk traverse equilibrium, has decreased by almost 200 ppm after 3000 years at 850°C. Second, local disequilibria between adjacent zones of the crystal may temporarily increase during trace element diffusion. For example, the Sr concentration at 392 μm initially increases relative to 443 μm , in spite of equilibrium partitioning requiring a lower Sr concentration at 392 μm relative to 443 μm . Maximum local disequilibrium between these two points is reached after ~ 250 years (see inset to Fig. 7). The reason for this local increase in disequilibrium is the high outflux of Sr from the high X_{An} (i.e. low equilibrium Sr) region at around 350 μm . This outflux cannot be dissipated quickly enough, resulting in temporary increases in local disequilibria in the surrounding regions.

As a first-order observation, however, it can be noted that for the bulk traverse, intracrystalline variations in Sr concentration increase over time by diffusion of Sr within the crystal. This increase in Sr variation can be used to infer crystal residence time at magmatic temperatures, as outlined below in more detail. It should be noted that diffusion of trace elements into or out of the section, either from the surrounding melt or from a third dimension, would promote a more rapid establishment of intracrystalline variations in Sr content, thereby yielding shorter residence times.

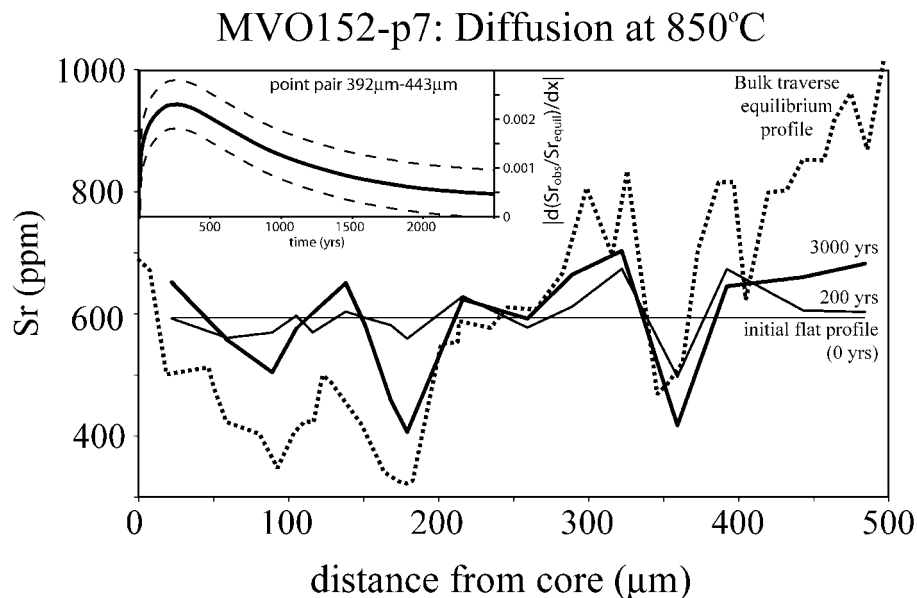


Fig. 7. Model showing the diffusive equilibration of an initially flat Sr profile towards bulk traverse equilibrium in plagioclase phenocryst MVO 152-p7 at 850°C. Inset: evolution of local Sr disequilibrium between the point pair 392 μm and 443 μm. (See Fig. 3 for method of calculating local disequilibrium.)

Crystal residence times at magmatic temperatures

Two-dimensional finite difference modelling of Sr diffusion has been applied to calculate crystal residence times at magmatic temperatures, 800–900°C in the case of the Montserrat andesites (Murphy *et al.*, 2000). Diffusion of an initially flat Sr profile, as suggested by crystallization modelling (see Fig. 5b), towards the variable bulk traverse equilibrium Sr profile was modelled using the finite difference method, until the standard deviation of modelled Sr concentrations around their average equalled the standard deviation of the observed Sr data. Standard deviations and calculated crystal residence times at 800°C, 850°C and 900°C are given in Table 1. Murphy *et al.* (2000) obtained temperatures of $858 \pm 18^\circ\text{C}$ and $861 \pm 16^\circ\text{C}$ from pyroxene geothermometry of the current and older Soufrière Hills andesites, so 850°C is considered a typical temperature. A temperature of 800°C was chosen as a lower limit for the existence of magma, because at this temperature the Soufrière Hills andesite would be almost completely solidified, based on phase equilibria constraints (Barclay *et al.*, 1998; Couch *et al.*, 2001). Although some reverse zoned orthopyroxene rims yield temperatures up to 1040°C (Murphy *et al.*, 2000), they are unlikely to have risen to above 900°C for significant periods of time, as $\sim 880^\circ\text{C}$ is the thermal stability limit of amphibole in the andesites (Barclay *et al.*, 1998). Thus, whereas the temperature of $\sim 850^\circ\text{C}$ is well constrained from crystal cores, 900°C is used as an

upper limit for the temperature of the andesite magma, whilst noting that very short-lived excursions to higher temperatures might have occurred as a result of a heating pulse by mafic magma influx. The range of 800–900°C provides useful sensitivity tests for the dependence of calculated residence times on temperature.

Some crystals have calcic cores with $X_{\text{An}} > 0.8$ (see Fig. 4a and f–h). As stated above, these cores may be restites from partial melting of the lower crust, remnants of an earlier phase of crystallization, or introduced into the andesite by mixing with mafic magma, and they are thus likely to be old. This is supported by the local equilibrium that these cores often display (Fig. 4f–h). However, as the diffusivity of Sr is very low in calcic plagioclase, the contribution of Sr from the cores to variations in the Sr profile does not have a significant effect on the residence timescales derived by diffusion modelling, which suggests that at 850°C crystal residence times range from a few years to a few hundred years. Residence times are independent of eruption age and, for the crystals studied from the current eruption, range from ~ 320 to ~ 17 years. Inspection of calculations at 800°C and 900°C (Table 1) shows that the inference of residence times of decades to centuries is not changed within the limits of reasonable magma temperatures. These estimates can be considered maxima, as some of the limited existing Sr variations may reflect small original variations recorded during crystal growth, i.e. not resulting from diffusion.

As an alternative interpretation, the crystals from the current eruption may have resided in their magma reservoir for the same time, but at different temperatures. A temperature range of $>100^{\circ}\text{C}$ would be required to account for the variable degrees of equilibration within the current eruption. Such temperature variations could be established only if crystals are removed from the hot interior of the convecting magma body to a cooler boundary layer. However, the average time for plagioclase crystals to be removed by crystal settling from a viscous convecting liquid such as the Montserrat magma exceeds 10^4 years (see Martin & Nokes, 1989), much longer than the timescales implied by the data presented here. Therefore, crystal residence times at magmatic temperatures are more likely to have been variable.

Discussion

The investigation of the detailed zoning patterns of plagioclase crystals places constraints on the processes and timescales of magma generation. Our data indicate that at Soufrière Hills there is no systematic increase of local disequilibria from the cores to the rims of plagioclase phenocrysts, and that crystallization was therefore rapid, taking a much shorter time than residence times of the crystals at magmatic temperatures. The latter range between ~ 10 years and a few hundred years at 850°C . The timescales of crystal residence at magmatic temperatures are much longer than the timescales of crystal growth, but are much shorter than the duration of intervals between episodes of major extrusive volcanism. Only six major domes are preserved over the last 175 ka (Harford *et al.*, 2002), and the stratigraphic record (Roobol & Smith, 1998) indicates short pulses of intense volcanism alternating with long periods of inactivity. Major episodes of andesite dome eruption appear to be relatively short-lived (periods of hundreds to thousands of years) and are separated by long periods of dormancy of the order of 10^4 years or more. For example, geochronological data indicate that there was a period of several eruptions from 24 to 16 ka, followed by dormancy of at least 12 kyr, before possible activity at 4 ka. The current eruption is the first major dome-forming event since 16 ka and was preceded by the small Castle Peak dome about 500 years ago.

A conventional model of magmatic systems envisages a shallow-level chamber that is cooling slowly, resulting in fractionation during periods of dormancy (Shaw, 1985). Our inferences of short residence times for plagioclase phenocrysts are inconsistent with the concept of a long-lived, slowly cooling shallow chamber of andesite existing below the Soufrière Hills for 75 kyr or more. Crystals in such a hypothetical chamber

should have grown very slowly and would have long residence times at high temperature. Our models suggest that in such a system most crystals would have attained bulk traverse equilibrium. Instead, the data suggest residence times of magma at high temperature for periods only of decades to centuries. Such short residence times suggest, in turn, that shallow magma chambers are ephemeral features.

The short timescales for crystallization pose problems for the model of a slowly cooling shallow and crystallizing magma body even if this magma body has a relatively short lifetime of a few centuries. In such circumstances, local Ba and Sr disequilibria in plagioclase phenocrysts should systematically increase from crystal cores to rims. Instead, local disequilibria are not systematic. This suggests that plagioclase crystallization is governed by rapid crystallization, followed by a longer period (decades to centuries) of residence involving very limited crystal growth. Data from the currently erupting lava indicate that the andesite has been remobilized from either completely solid or partially molten material recently by the influx of hydrous basalt (Devine *et al.*, 1998; Murphy *et al.*, 2000; Harford & Sparks, 2001). Although the remobilization concept can explain many of the heterogeneities and disequilibrium features in the andesite, this model does not elucidate the entire crystallization history of the andesite. The phenocryst assemblage of plagioclase, amphibole, orthopyroxene and oxide must have formed during earlier shallow-level crystallization events. The large plagioclase phenocrysts investigated here form part of this earlier episode. These disparate observations and constraints can be reconciled by the model shown in Fig. 8. Here, hydrous andesite melt (≥ 5 wt % H_2O) is generated by crystallization of hydrous basalt magma in the deep crust (Zellmer *et al.*, 2003). The andesite melt separates from the source region and ascends into the upper crust. On reaching depths of a few kilometres, these wet magmas become gas saturated and undergo spontaneous and rapid crystallization as they degas (Blundy & Cashman, 2001). Degassing is an attractive way of inducing crystallization and solidification on a very short timescale. Furthermore, degassing-induced crystallization causes viscosity to increase dramatically so that magmas stall at depths of a few kilometres.

The plagioclase zoning patterns, however, are too complex to have formed in a single batch of magma emplaced, degassed and crystallized in one episode. Large changes in anorthite content are difficult to reconcile with changes in P_{total} or $P_{\text{H}_2\text{O}}$ in a magma chamber where pressure fluctuations are only a small fraction of total pressure. Reversals, zones of resorption and partial resorption, and variable apparent crystal residence times indicate a multistage, pulsatory

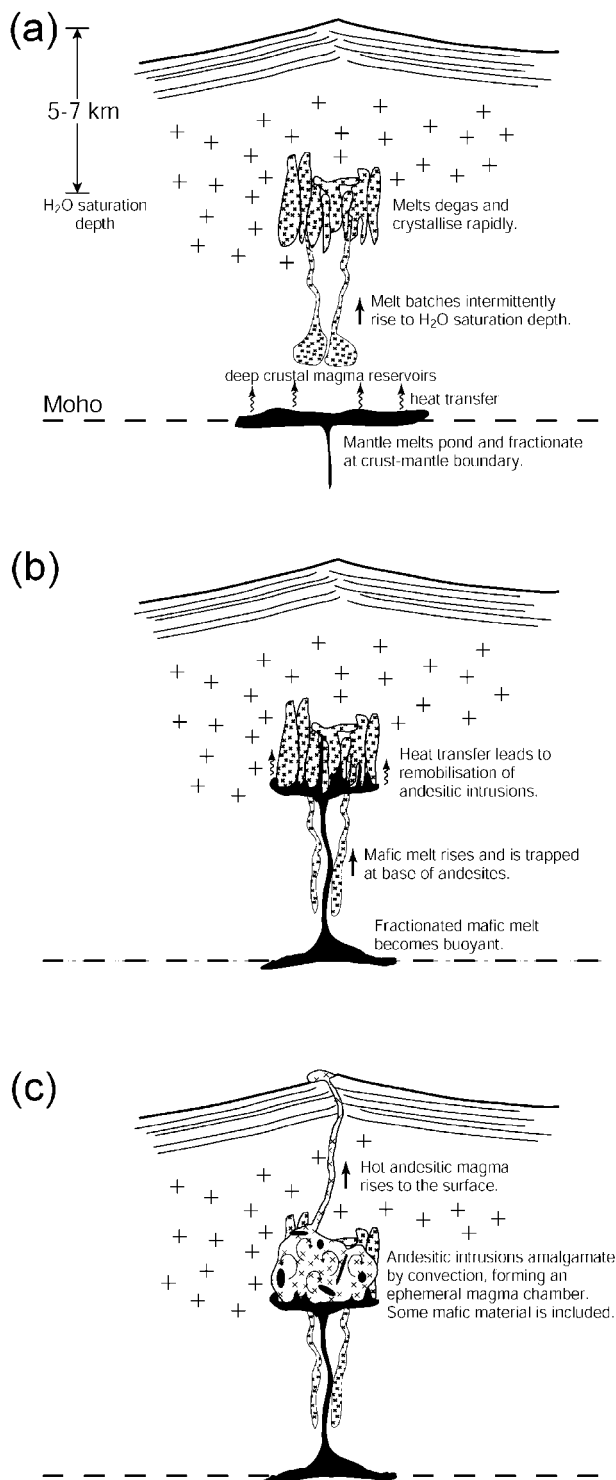


Fig. 8. Petrogenetic model for the Montserrat andesites. (a) Lower-crustal fractionation follows ponding of mafic magma at the Moho. Andesitic melt batches intermittently rise to their H₂O saturation depth (5–7 km), where they degas and rapidly crystallize. (b) Mafic magma becomes buoyant and rises to the base of the andesitic intrusives. (c) The andesites amalgamate, mix with some of the mafic magma, and erupt. The mafic material is sampled at the surface as inclusions of mafic magma within the andesite.

history. These patterns can be interpreted in the context of the recent activity of the volcano. The rise of andesite magma to high levels can be traced back at least to the eruption of the small ($5 \times 10^7 \text{ m}^3$) dome of Castle Peak 500 years ago. The volcano-seismic crises of 1896–1897, 1933–1937 and 1966–1967 (MacGregor, 1938; Perret, 1939; Shepherd *et al.*, 1971) can be interpreted as rise of andesite magma that failed to erupt. Taken together with the 1995–2001 eruption, magma rise was pulsatory with an ~ 30 year timescale. This history may be interpreted as the pulsatory emplacement of andesitic magma into the shallow crust. In this model the magma reservoir is a small ephemeral feature that cools rapidly and may not erupt. As the mass of magma in the upper crust increases with each successive pulse of andesite, the system approaches eruption conditions. The recent influx of hydrous mafic magma has provided sufficient heat to remobilize the previously intruded andesites. The development of the current magma reservoir is reflected in the complex plagioclase zoning patterns. The timescales of crystal residence at high temperature are decades to centuries, and are similar to the timescales of magma emplacement leading to the current activity.

We propose a model where andesite magmas reside in the deep crust and rise episodically to form ephemeral upper-crustal chambers, which feed periods of intense volcanism during their short existence. Basaltic magmas are continuously supplied to the crust beneath Montserrat, where they pond and thermally equilibrate to generate hydrous andesite melts (Zellmer *et al.*, 2003). The production of similar andesite magmas throughout the history of Soufrière Hills implies a thermally buffered system of temperatures around 850–900°C. We propose that melts are stored in these deep source zones until buoyancy becomes sufficient to induce magma ascent. The hydrous andesites rise and start crystallizing in the upper crust, where they become water oversaturated. The rising magmas then stall as their viscosity increases, and ephemeral magma chambers start to develop, as described above. Such shallow chambers continue to develop and erupt until the deep supply is exhausted. The system returns to dormancy until the deep system accumulates enough melt, source rock and buoyancy to initiate a new cycle.

CONCLUSIONS

Nomarski interference contrast images and variations in major element composition of plagioclase phenocrysts from the Soufrière Hills volcano, Montserrat, Lesser Antilles, reveal complex growth histories and are consistent with the concepts of periodic magma heating and remobilization.

Intracrystalline variations in local Sr and Ba disequilibria in plagioclase phenocrysts constrain the duration of crystal growth and residence. In the Soufrière Hills andesites, local disequilibria do not systematically increase towards crystal rims, suggesting that crystal growth occurred over a short period compared with crystal residence times at magmatic temperatures.

Observed Sr profiles are approximately flat, consistent with the combined opposing effects of anorthite content on Sr partitioning between plagioclase and melt, and of fractionation on melt X_{An} and Sr composition. After crystallization, the Sr zonation should increase, reflecting equilibration with the X_{An} zonation. However, the observed Sr zonation is minor, suggesting limited crystal residence times at magmatic temperatures.

Plagioclase phenocryst residence times at 850°C were calculated using two-dimensional finite difference modelling of diffusion of an initially flat Sr profile towards the observed profile, with both equilibrium partitioning and diffusion coefficients varying across each crystal as a result of the dependence of these parameters on anorthite content. Residence times range from ~10 years to a few hundred years in 12 crystals of six samples from prehistoric and currently erupting andesites.

Complex crystal growth histories, rapid crystal growth, and variable crystal residence time can be reconciled if small volumes of andesite are intermittently intruded into the upper crust, where they rapidly crystallize as a result of degassing. Subsequent influx of mafic magma leads to an amalgamation of these andesitic intrusives by convective processes, ultimately leading to eruption. Magma residence times are short compared with the longevity of the volcano, and this is consistent with generation and long-term storage of andesite deep in the crust. Episodic ascent of deeply stored magma leads to formation of ephemeral magma reservoirs and episodes of intense volcanic activity.

ACKNOWLEDGEMENTS

We would like to thank the Montserrat Volcano Observatory (MVO) for fieldwork support. Nomarski imaging was performed at Geneva University, and we would like to thank Michael Dungan for supplying the facilities and Fidel Costa for an introduction to this technique. Stuart Kearns and Richard Brooker provided help with the electron microprobe analyses, and Richard Hinton's continued support at the Edinburgh ion microprobe facility is very much appreciated. Jörg Erzinger is thanked for providing access to the GFZ ion microprobe facility and for his general support, and Dieter Rhede for insights into the primary column. The AMNH 95557 reference sample used in Potsdam

was provided by the American Museum of Natural History. Laser ablation inductively coupled plasma mass spectrometry data for this sample were kindly provided by Peter Dulski. The constructive comments of Catherine Annen, Ilya Bindemann, Jon Blundy, Tim Elliott, Chloe Harford, Oleg Melnik, Richie Robertson and Simon Turner improved this manuscript. We also thank Christian Herrmann, Günter Hofmann, and Dirk and August Ihrig for their support. Constructive comments by Stephen Blake and an anonymous reviewer substantially improved the manuscript. Ion microprobe analyses in Edinburgh were funded by NERC (IMP/159/0400). G.F.Z. was funded by a Leverhulme Research Grant (F/182/BI) and a DFG travel grant (ZE492/1-1) to work at the GeoForschungsZentrum. R.S.J.S. was funded by an NERC fellowship.

SUPPLEMENTARY DATA

For supplementary data, please refer to *Journal of Petrology* Online.

REFERENCES

- Anderson, A. T., Jr (1983). Oscillatory zoning of plagioclase: Nomarski interference contrast microscopy of etched polished sections. *American Mineralogist* **68**, 125–129.
- Anderson, A. T., Jr (1984). Probable relations between plagioclase zoning and magma dynamics, Fuego Volcano, Guatemala. *American Mineralogist* **68**, 660–676.
- Barclay, J., Rutherford, M. J., Carroll, M. R., Murphy, M. D., Devine, J. D., Gardner, J. & Sparks, R. S. J. (1998). Experimental phase equilibria constraints on pre-eruptive storage conditions of the Soufrière Hills magma. *Geophysical Research Letters* **25**, 3437–3440.
- Barmin, A., Melnik, O. & Sparks, R. S. J. (2002). Periodic behaviour in lava dome eruptions. *Earth and Planetary Science Letters* **199**, 173–184.
- Blundy, J. & Cashman, K. (2001). Ascent-driven crystallisation of dacite magmas at Mount St Helens, 1980–1986. *Contributions to Mineralogy and Petrology* **140**, 631–650.
- Blundy, J. D. & Wood, B. J. (1991). Crystal-chemical controls on the partitioning of Sr and Ba between plagioclase feldspar, silicate melts, and hydrothermal solutions. *Geochimica et Cosmochimica Acta* **55**, 193–209.
- Burnham, C. W. (1975). Water and magmas; a mixing model. *Geochimica et Cosmochimica Acta* **39**, 1077–1084.
- Charlier, B. L. A. & Zellmer, G. F. (2000). Some remarks on U–Th mineral ages from igneous rocks with prolonged crystallisation histories. *Earth and Planetary Science Letters* **183**, 457–469.
- Cherniak, D. J. & Watson, E. B. (1994). A study of strontium diffusion in plagioclase using Rutherford backscattering spectroscopy. *Geochimica et Cosmochimica Acta* **58**, 5179–5190.
- Condomines, M. (1997). Dating recent volcanic rocks through ^{230}Th – ^{238}U disequilibrium in accessory minerals: example of the Puy de Dome (French Massif Central). *Geology* **25**, 375–378.

- Couch, S., Sparks, R. S. J. & Carroll, M. R. (2001). Mineral disequilibrium in lavas explained by convective self-mixing in open magma chambers. *Nature* **411**, 1037–1039.
- Devine, J. D., Murphy, M. D., Rutherford, M. J., Barclay, J., Sparks, R. S. J., Carroll, M. R., Young, S. R. & Gardner, J. E. (1998). Petrologic evidence for pre-eruptive pressure–temperature conditions, and recent reheating, of andesitic magma erupting at the Soufriere Hills Volcano, Montserrat, W. I. *Geophysical Research Letters* **25**, 3669–3672.
- Devine, J. D., Rutherford, M. J., Norton, G. E. & Young, S. R. (2003). Magma storage region processes inferred from geochemistry of Fe–Ti oxides in andesitic magma, Soufrière Hills Volcano, Montserrat, W.I. *Journal of Petrology* **44**, 1375–1400.
- Giletti, B. J. & Casserly, J. E. D. (1994). Strontium diffusion kinetics in plagioclase feldspars. *Geochimica et Cosmochimica Acta* **58**, 3785–3793.
- Harford, C. L. & Sparks, R. S. J. (2001). Recent remobilization of shallow-level intrusions on Montserrat revealed by hydrogen isotope composition of amphiboles. *Earth and Planetary Science Letters* **185**, 285–297.
- Harford, C. L., Pringle, M. S., Sparks, R. S. J. & Young, S. R. (2002). The volcanic evolution of Montserrat using $^{40}\text{Ar}/^{39}\text{Ar}$ geochronology. In: Druitt, T. H. & Kokelaar, B. P. (eds) *The Eruption of the Soufriere Hills Volcano, Montserrat, from 1995 to 1999*. Geological Society, London, Memoir **21**, 664 pp.
- Hawkesworth, C. J., Blake, S., Turner, S. P. & Thomas, L. E. (2001). Magma differentiation rates: combining isotopic constraints and thermal models. *EOS Transactions, American Geophysical Union* **82**, 261–265.
- Higgins, M. D. (1996). Magma dynamics beneath Kameni volcano, Thera, Greece, as revealed by crystal size and shape measurements. *Journal of Volcanology and Geothermal Research* **70**, 37–48.
- Hinton, R. W. (1990). Ion microprobe trace-element analysis of silicates: measurement of multi-element glasses. *Chemical Geology* **83**, 11–25.
- Holman, J. P. (1997). *Heat Transfer*. New York: McGraw–Hill.
- Housh, T. B. & Luhr, J. F. (1991). Plagioclase–melt equilibria in hydrous systems. *American Mineralogist* **76**, 477–492.
- MacGregor, A. G. (1938). The Royal Society Expedition to Montserrat, B. W. I. The volcanic history and petrology of Montserrat with observations on Mt Pelée, in Martinique. *Philosophical Transactions of the Royal Society of London, Series B* **229**, 1–90.
- Martin, D. & Nokes, R. (1989). A fluid-dynamical study of crystal settling in convecting magmas. *Journal of Petrology* **30**, 1471–1500.
- Morse, S. A. (1984). Cation diffusion in plagioclase feldspar. *Science* **225**, 504–505.
- Murphy, M. D., Sparks, R. S. J., Barclay, J., Carroll, M. R., Lejeune, A.-M., Brewer, T. S., Macdonald, R., Black, S. & Young, S. (1998). The role of magma mixing in triggering the current eruption at the Soufriere Hills volcano, Montserrat, West Indies. *Geophysical Research Letters* **25**, 3433–3436.
- Murphy, M. D., Sparks, R. S. J., Barclay, J., Carroll, M. R. & Brewer, T. S. (2000). Remobilization of andesite magma by intrusion of mafic magma at the Soufriere Hills volcano, Montserrat, West Indies. *Journal of Petrology* **41**, 21–42.
- Pailuc, G. (1932). Untersuchungen der Plagioklase einiger tertiärer Ergussgesteine Siebenbürgens (Rumänien) mittelst der Unversaldrehtischmethode. *Schweizerische Mineralogische und Petrologische Mitteilungen* **12**, 423–444.
- Perret, F. A. (1939). The volcano-seismic crisis at Montserrat, 1933–1937. *Publications of the Carnegie Institution, Washington* **512**, 1–76.
- Powell, C. F. (1938). The Royal Society expedition to Montserrat, B. W. I. Final report. *Philosophical Transactions of the Royal Society, Series A* **237**, 1–34.
- Roobol, M. J. & Smith, A. L. (1998). Pyroclastic stratigraphy of the Soufriere Hills volcano, Montserrat—implications for the present eruption. *Geophysical Research Letters* **25**, 3393–3396.
- Shaw, H. R. (1985). Links between magma-tectonic rate balances, plutonism, and volcanism. *Journal of Geophysical Research* **90**, 11275–11288.
- Shepherd, J. B., Tomblin, J. F. & Woo, D. A. (1971). Volcano-seismic crisis in Montserrat, West Indies, 1966–67. *Bulletin of Volcanology* **35**, 143–163.
- Singer, B. S., Pearce, T. H., Kolisnik, A. M. & Myers, J. D. (1993). Plagioclase zoning in mid-Pleistocene lavas from the Segua volcanic center, central Aleutian arc, Alaska. *American Mineralogist* **78**, 143–157.
- Singer, B. S., Dungan, M. A. & Layne, G. D. (1995). Textures and Sr, Ba, Mg, Fe, K, and Ti compositional profiles in volcanic plagioclase: clues to the dynamics of calc-alkaline magma chambers. *American Mineralogist* **80**, 776–798.
- Stamatelopoulou-Seymour, K., Vlassopoulos, D., Pearce, T. H. & Rice, C. (1990). The record of magma chamber processes in plagioclase phenocrysts at Thera Volcano, Aegean Volcanic Arc, Greece. *Contributions to Mineralogy and Petrology* **104**, 73–84.
- Stewart, M. L. & Fowler, A. D. (2001). The nature and occurrence of discrete zoning in plagioclase from recently erupted andesitic volcanic rocks, Montserrat. *Journal of Volcanology and Geothermal Research* **106**, 243–253.
- Tait, S., Jaupart, C. & Vergnolle, S. (1989). Pressure, gas content and eruption periodicity of a shallow, crystallizing magma chamber. *Earth and Planetary Science Letters* **92**, 107–123.
- Yoder, H. S., Stewart, D. B. & Smith, J. R. (1957). Ternary feldspars. *Carnegie Institution of Washington, Yearbook* **56**, 206–214.
- Zellmer, G. F., Blake, S., Vance, D., Hawkesworth, C. & Turner, S. (1999). Plagioclase residence times at two island arc volcanoes (Kameni islands, Santorini, and Soufriere, St. Vincent) determined by Sr diffusion systematics. *Contributions to Mineralogy and Petrology* **136**, 345–357.
- Zellmer, G. F., Hawkesworth, C. J., Sparks, R. S. J., Thomas, L. E., Harford, C. L., Brewer, T. S. & Loughlin, S. C. (2003). Geochemical evolution of the Soufrière Hills volcano, Montserrat, Lesser Antilles volcanic arc. *Journal of Petrology* **44**, 1349–1374.
- Zinner, E. & Crozaz, G. (1986). A method for the quantitative measurement of rare earth elements in the ion microprobe. *International Journal of Mass Spectrometry and Ion Processes* **69**, 17–38.